DOI: 10.19884/j.1672-5220.202503001

Effect of Substrate Temperature on Preparation of SiO_2-like Thin Films by Plasma Jet

ZHANG Jiaojiao[1], XU Yu[1, 2, 3*], QIAN Zhixin[1], HUANG Xiaojiang[1, 2, 3]
1. College of Physics, Donghua University, Shanghai 201620, China
2. Member of Magnetic Confinement Fusion Research Center, Ministry of Education, Donghua University, Shanghai 201620, China
3. Textiles Key Laboratory for Advanced Plasma Technology and Application, Donghua University, Shanghai 201620, China

Abstract: This study explores the effects of the substrate temperature (25–200 ℃) on SiO_2-like thin films prepared via atmospheric-pressure plasma jet. Films deposited at elevated temperatures exhibited a reduced thickness (from 242 to 156 nm) but enhanced mechanical and chemical performance. The pencil hardness improved from grade B to 4H. The adhesion reached class 0 (no detachment) at temperatures of 100 ℃ and above. X-ray photoelectron spectroscopy (XPS) confirmed carbon reduction and silicon dioxide (SiO_2) enrichment when the substrate temperature increased from 25 to 200 ℃, indicating intensified precursor decomposition. Hydrochloric acid corrosion testing (3.0 h immersion) revealed that the films deposited at 200 ℃ exhibited improved corrosion resistance, with a mass loss of 6.53% compared to 7.01% for the bare substrates. The results indicate that the substrate temperature is a critical process parameter for preparing protective films applied in corrosive environments.

Keywords: atmospheric-pressure plasma jet; discharge; thin film; substrate temperature; corrosion resistance; SiO_2
CLC number: O539 **Document code**: A
Article ID: 1672-5220(2026)04-0026-08

0 Introduction

The escalating demands of modern industrial applications impose progressively stringent requirements on material surface performance, particularly under extreme operational conditions involving thermal, corrosive, and mechanical stresses[1-2]. While stainless steel remains a critical structural material for acid-handling infrastructure (e.g., pipelines and reactors in fossil fuel exhaust systems), its inherent vulnerability to hydrochloric acid (HCl) corrosion necessitates advanced surface protection strategies. Silicon dioxide (SiO_2) films have emerged as quintessential protective films due to their exceptional hardness (a Mohs hardness of 7–8), superior chemical stability, and thermal resistance exceeding 1 600 ℃, making them ideal candidates for prolonging substrate longevity in aggressive environments[3-5].

Recent advancements demonstrate the multifunctional efficacy of SiO_2 films across diverse domains. Yang et al.[6] developed sol-gel-derived organic-inorganic composite films that enhanced brick weather resistance by 42%, while Xie et al.[7] achieved a 68% improvement in iron fiber oxidation resistance through silica surface modification. Such films also exhibit cross-industry potential, from scratch-resistant automotive finishes to UV-stable architectural films.

SiO_2 deposition techniques include dip-coating[8-9], magnetron sputtering[10], and liquid-phase deposition[11]. Despite methodological progress in these techniques, persistent limitations in film uniformity, deposition efficiency, and scalability hinder their industrial adoption. Plasma has been increasingly employed in the preparation and treatment of materials[12-13]. Plasma jet technology has gained prominence due to its non-line-of-sight deposition capability, rapid growth rates, and superior interfacial adhesion. However, since the macroscopic performance of plasma-deposited SiO_2 films is highly dependent on their microstructure, even minor variations in substrate temperature can critically alter crystallographic orientation, defect density, and stoichiometric composition[14-15].

This study investigates the effect of substrate temperature on plasma jet-deposited SiO_2 film performance. A series of SiO_2-like thin films were fabricated through systematic substrate temperature regulation. The temperature-dependent evolution of film microstructure and macroscopic properties was systematically investigated through surface morphology

Received date: 2025-03-03
Foundation item: National Outstanding Youth Science Foundation, China (No. 12205040)
* Correspondence should be addressed to XU Yu, email: yuxu@dhu.edu.cn
Citation: Zhang J J, Xu Y, Qian Z X, et al. Effect of substrate temperature on preparation of SiO_2-like thin films by plasma jet[J]. *Journal of Donghua University (English Edition)*, 2026, 43(4): 26-33.

characterization (by scanning electron microscopy, SEM), compositional profiling (by X-ray photoelectron spectroscopy, XPS), mechanical property assessments (by pencil hardness and cross-cut adhesion tests), and HCl corrosion testing.

1 Materials and Methods

1.1 Reagents and instruments

Hexamethyldisiloxane (HMDSO) was purchased from Adamas Reagents Co., Ltd., Shanghai, China. HCl was obtained from Sinopharm Chemical Reagents Co., Ltd., Shanghai, China. Argon gas with a purity of 99.995% was supplied by Shanghai Haoqi Gas Co., Ltd., Shanghai, China. Oxygen gas with a purity of 99.995% was supplied by Shanghai Shenzhong Gas Co., Ltd., Shanghai, China.

HMDSO was heated in an HH-1 thermostatic water bath (Tianrui, Changzhou, China) at 40 ℃. The substrate was heated on an XKWKQ-A-1 heating block (Xuankang, Xinghua, China). The gas flow was regulated using CS200A mass flow controllers (Sevenstar, Beijing, China). The discharge was generated using an RSG500S 13.56 MHz low-temperature plasma source (Rishige, Changzhou, China).

1.2 Experimental setup

The HMDSO precursor, existing as a liquid at ambient temperature, was loaded into a bubbler and maintained at 40 ℃ within a thermostatic water bath throughout the experimental process. The experimental setup (Fig. 1) employed a dual-gas delivery system: a primary argon stream functioned as the carrier gas, transporting vaporized HMDSO from the bubbler into the central copper tube, while a secondary argon stream served as the discharge gas, which was precisely mixed with oxygen through mass flow controllers before being introduced into the reaction chamber's side inlet. The reaction chamber comprises a custom-designed quartz glass tube featuring a sealed upper section and an open lower configuration. A lateral inlet port is incorporated for the controlled introduction of argon and oxygen mixtures through the delivery tubing system. A hollow copper tube is positioned centrally, with an open upper end for the intake of HMDSO and a closed lower end. The base of the tube features eight evenly distributed circular holes, each with a diameter of 1 mm, through which HMDSO is delivered to the discharge region. The experiment utilized a 13.56 MHz radiofrequency power source, which was modulated by an impedance matcher and applied to the copper electrode surrounding the exterior of the glass tube. The central copper tube was grounded, and the region between the glass tube and the copper tube served as the discharge area. The substrate was positioned 2 mm from the jet exit and placed together with the heater on a movable platform.

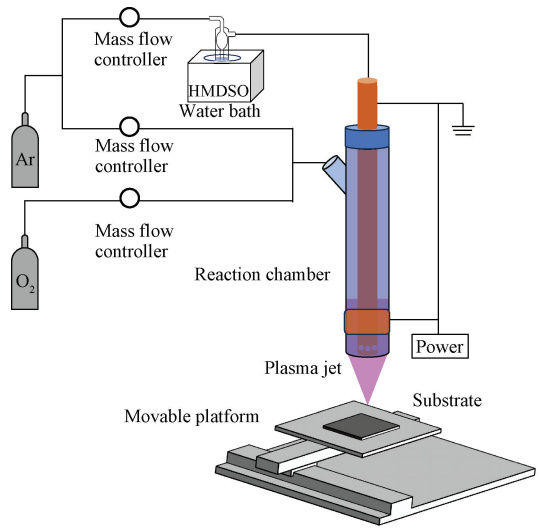


Fig. 1 Experimental setup

1.3 Experimental scheme

The radiofrequency power source was set at 40 W, with flow rates of Ar, O_2, and HMDSO adjusted to 1 000, 1, and 40 standard cubic centimeters per minute (sccm), respectively. The movable platform was configured to translate at a speed of 1 cm/s. Single-crystal silicon wafers were employed as substrates. The heater parameters were adjusted to conduct experiments at substrate temperatures of 25, 50, 100, 150, and 200 ℃, and the corresponding samples were termed S25, S50, S100, S150, and S200, respectively.

1.4 Performance characterization

The mass of the substrate was measured using an ME204E electronic balance (METTLER TOLEDO, Shanghai, China). The voltage and current curves were obtained using a combination of P6015A voltage probe (Tektronix, Beaverton, USA), P2877 current probe (Pearson Electronics, Boulder, USA), and SDS2504X HD digital oscilloscope (Siglent, Shenzhen, China). The species information in the discharge area was analyzed using an AvaSpec-2048TEC spectrometer (AVANTES, Apeldoorn, the Netherlands). The cross-sectional thickness of the film was observed using an S-4800 scanning electron microscope (Hitachi, Tokyo, Japan). The film composition was analyzed using an Escalab 250Xi X-ray photoelectron spectrometer (Thermo Fisher, Waltham, USA). The film hardness was tested using a pencil hardness tester (Huaguo, Dongguan, China). The film hardness was evaluated in accordance with the standard GB/T 6739—2022. Wooden drawing pencils with a hardness grade range of 6B to 6H were prepared, and their tips were ground vertically flat using sandpaper. The pencils were then mounted on a pencil hardness tester with a 750 g load, with the pencil tips forming a 45° angle with the sample. The pencil hardness tester was subsequently pushed. After completing the hardness tests, the film was examined by a microscope

for any signs of damage. The highest hardness grade at which the film remained intact was designated as the pencil hardness of the film. The adhesion of the film was characterized by ethanol wiping tests and cross-cut tests. The adhesion of the film was evaluated in accordance with the standard GB/T 9286—2021, where class 0 represents the highest adhesion level characterized by smooth edges and no detachment, and class 1 indicates slight detachment at the intersections of the cuts. The test required placing the specimen on a rigid, flat surface and making six horizontal and six vertical cuts with a pitch of 1 mm between adjacent cuts, penetrating to the substrate to form 25 individual squares. A pressure-sensitive adhesive tape was then applied to completely cover the grid, ensuring firm contact. Within 5 min after applying the tape, the tape was smoothly removed at an angle of approximately 60°. The detached area of the film was subsequently evaluated under a scanning electron microscope. The corrosion resistance of the film was characterized by conducting corrosion experiments on stainless steel substrates after coating.

2 Results and Discussion

2.1 Plasma characteristics

Figure 2 shows the voltage and current curves of the discharge at a power supply setting of 40 W. It can be observed that both curves are sinusoidal, with the current phase leading the voltage phase by approximately 133°, indicating that the discharge is a typical capacitive discharge[16]. The information in Fig. 2 indicates that the discharge has a peak-to-peak voltage of 1 196 V and a peak-to-peak current of 0.42 A, with a discharge frequency of 13.56 MHz, which is consistent with the experimental settings.

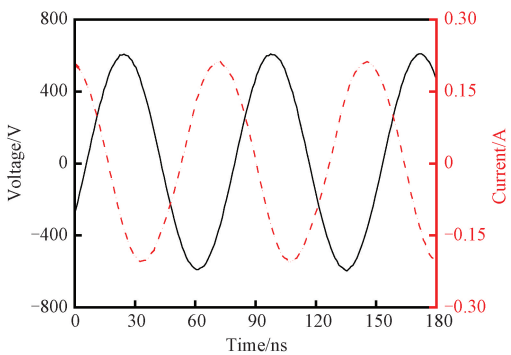


Fig. 2 Voltage and current curves of discharge

The spectral diagnostic method was applied to analyze key species information in the plasma discharge region. Under the experimental conditions described in Subsection 1.2, spectral lines were collected during discharge. While maintaining other parameters unchanged, the discharge gas was replaced with pure argon for comparative spectral acquisition. The comparison results are shown in Fig. 3. The spectral intensity of nitrogen exhibits a decrease compared with that of pure argon discharge. This reduction is attributed to chemical reactions induced by HMDSO addition, which consumed partial energy and weakened nitrogen ionization. Additionally, the silicon spectral line at 251.6 nm was detected, confirming precursor decomposition and indicating the feasibility of SiO_2 synthesis.

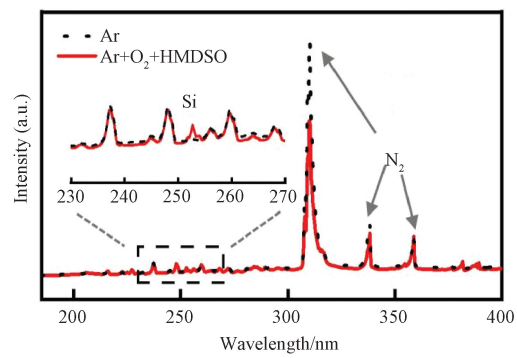


Fig. 3 Spectrum measurement results

2.2 Mechanical properties

The movable platform was fixed, and single-crystal silicon wafers were used as substrates for 2-min static deposition at different temperatures. The results are shown in Fig. 4. As the substrate temperature increases, the deposited spot patterns shrink, and the film thickness decreases, consistent with a reduced growth rate at higher temperatures. To evaluate the adhesion strength, the coated surfaces were subsequently sprayed with ethanol and wiped. The extent of pattern removal gradually diminished with rising substrate temperature, and at 200 ℃, the patterns remained virtually unchanged after wiping. Given that the reduced thickness would intuitively facilitate easier removal, this resistance to ethanol wiping strongly suggests a significant enhancement in interfacial adhesion at elevated temperatures[17].

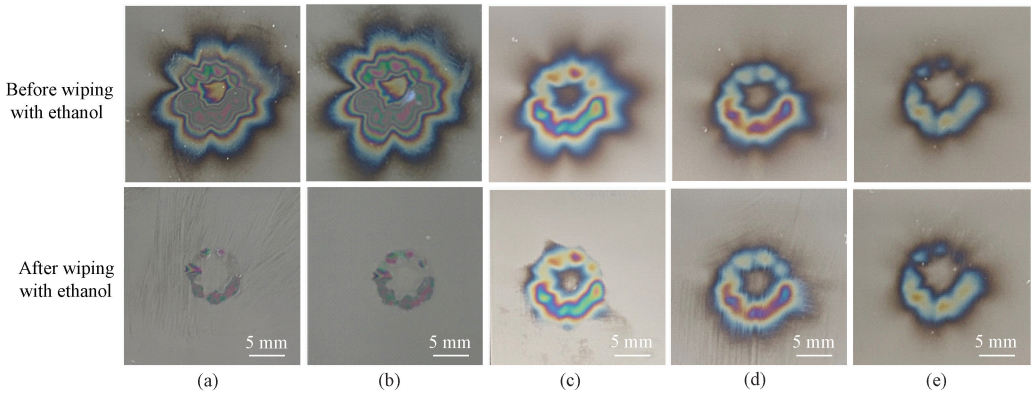


Fig. 4 Patterns before and after wiping with ethanol at different substrate temperatures: (a) 25 ℃; (b) 50 ℃; (c) 100 ℃; (d) 150 ℃; (e) 200 ℃

To further characterize the adhesion of the films, dynamic film deposition was performed by activating the movable platform, and cross-cut tests were conducted on samples deposited at different temperatures. The test results are shown in Fig. 5. It can be observed that samples fabricated at 25 and 50 ℃ exhibit distinct notches, with an adhesion class of 1, whereas the samples fabricated at other temperatures remain intact, achieving an adhesion class of 0.

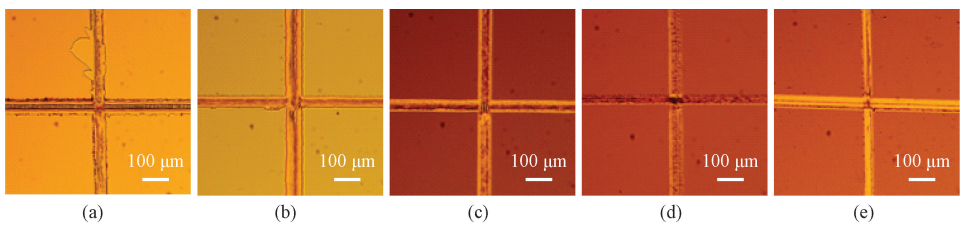


Fig. 5 Cross-cut test results at different substrate temperatures: (a) 25 ℃; (b) 50 ℃; (c) 100 ℃; (d) 150 ℃; (e) 200 ℃

If the film merely adheres to the substrate through van der Waals interactions, it generally fails the hardness test[18]. The hardness of the film is summarized in Table 1, which shows a significant increase in hardness with increasing substrate temperature. Enhancing the kinetic energy of adsorbed atoms by elevating the substrate temperature during deposition promotes better reorganization and agglomeration of these atoms, resulting in higher density. This, in turn, is reflected in the progressively increasing hardness of the film.

Table 1 Mechanical properties of films

Temperature/℃	Pencil hardness grade	Cross-cut adhesion class
25	B	1
50	HB	1
100	H	0
150	3H	0
200	4H	0

2.3 Film thickness and composition

The cross-section of the film was observed using a scanning electron microscope, as shown in Fig. 6. To ensure the accuracy of the data, three random points were selected on the image to measure the film thickness, and the average was calculated. The film thickness gradually decreased with increasing substrate temperature, consistent with the trend obtained from the stationary deposition (Fig. 4), where an increase in substrate temperature led to a reduction in the film growth rate. This is because elevated temperatures not only accelerate the forward deposition reaction but also promote the reverse reaction (e.g., etching or decomposition of the deposited SiO_2 species), thus reducing the growth rate of the film[19]. The increased substrate temperature can increase the mobility of surface atoms and promote the diffusion and reaction of adsorbed species, and thus a more stable surface structure forms. However, high temperature tends to reduce the residence time of the adsorbed species, which may lead to the detachment of some active species from the surface before the reaction, thereby reducing the deposition rate[20].

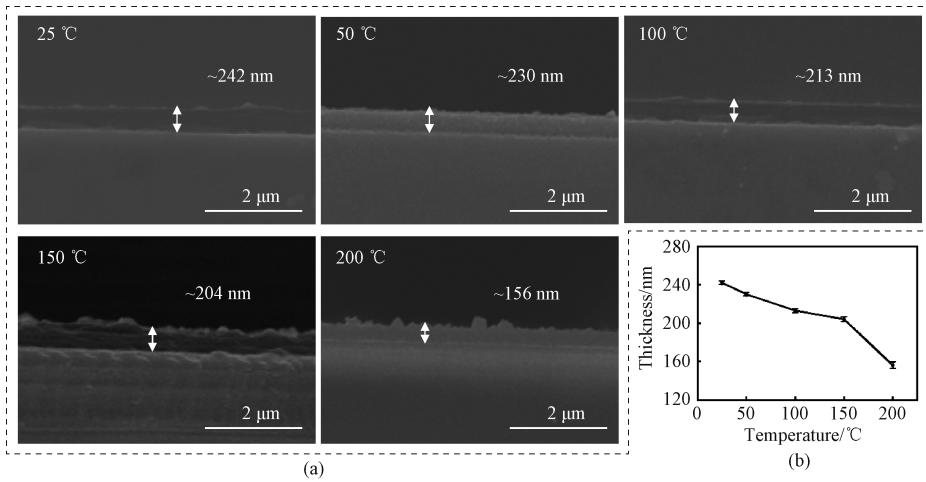


Fig. 6 Cross-sectional morphologies of SiO_2-like thin films prepared at different substrate temperatures: (a) SEM images; (b) film thickness derived from SEM images as a function of substrate temperature

The chemical composition of the film was analyzed by XPS. The corresponding survey spectra are displayed in Fig. 7, and the derived atomic percentages of the constituent elements (e.g., Si, O, and C) on the films are summarized in Table 2. The C—O—C bond is formed when methyl radicals, released from HMDSO cleavage, react with oxygen. According to the comparison of data at 25 and 200 ℃ in Table 2, as the substrate temperature increases, the atomic percentages of Si and O increase from 32.9% to 34.4% and from 43.9% to 50.4%, respectively, while that of C decreases from 23.2% to 15.2%. The results indicate that the elevated substrate temperature promotes more complete pyrolysis of the organic precursor. This is attributed to the enhanced thermal motion of precursor molecules, which facilitates bond cleavage and generates reactive fragments that readily interact with plasma-active species to form SiO_2.

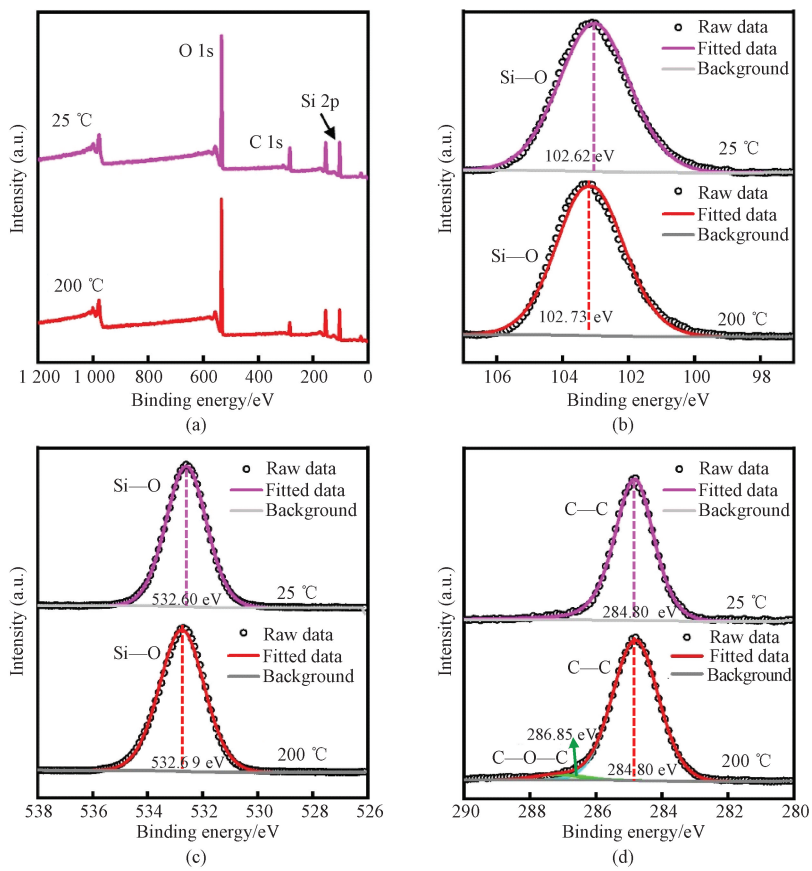


Fig. 7 XPS spectra of SiO_2-like thin films: (a) full spectra; (b) Si 2p spectra; (c) O 1s spectra; (d) C 1s spectra

Table 2 Atomic percentages of elements

Temperature/℃	Atomic percentage/%		
	C	Si	O
25	23.2	32.9	43.9
200	15.2	34.4	50.4

2.4 Corrosion testing results

This study used the immersion coupon method to investigate the corrosion behavior of samples in HCl solutions at varying temperatures. Customized 304 stainless steel plates (50 mm × 20 mm × 2 mm) were prepared with 3-mm-diameter holes at identical positions for suspension during immersion tests. The surfaces were mechanically polished with sandpaper and subsequently ultrasonically cleaned in acetone, ethanol, and deionized water for 10 min each to eliminate organic contaminants, and then dried in an oven. The prepared steel plates were mounted on a custom-designed movable platform for dynamic film deposition. The deposited steel plates were allowed to cool to room temperature. A set of uncoated steel plates served as a control group. The mass of each steel plate was measured and recorded using a microbalance.

The HCl solution (a mass fraction of 10.5%) was prepared and placed in a water bath maintained at 60 ℃. The steel plates were suspended on a rack to ensure full immersion of their surfaces in the HCl solution. After immersion for 1.5 h and 3.0 h, respectively, the steel plates were removed, ultrasonically cleaned, dried, and weighed.

The experimental results in Table 3 show that the mass loss decreases as the substrate temperature increases. The increase in the substrate temperature facilitates the diffusion of atoms deposited on the substrate surface, enabling them to recombine more readily and repair defects within the film, thereby enhancing the film density and achieving improvement in corrosion resistance.

Table 3 Mass changes of samples before and after HCl immersion

Sample	Mass/g			Mass loss (after immersion for 3.0 h)/g	Mass loss ratio (after immersion for 3.0 h)/%
	Before immersion	After immersion for 1.5 h	After immersion for 3.0 h		
Control	15.318 2	14.649 5	14.244 3	1.073 9	7.01
S25	15.327 9	14.687 2	14.262 9	1.065 0	6.95
S50	15.296 9	14.664 3	14.237 7	1.059 2	6.92
S100	15.319 1	14.680 9	14.253 6	1.065 5	6.96
S150	15.306 8	14.705 2	14.256 4	1.050 4	6.86
S200	15.316 6	14.720 2	14.317 0	0.999 6	6.53

3 Conclusions

The plasma jet technology was employed to deposit SiO_2-like thin films on substrate surfaces and the effects of the substrate temperature on film performance were systematically investigated. A series of thin film samples were prepared with substrate temperatures ranging from 25 to 200 ℃, at a fixed power supply of 40 W and an Ar/O_2/HMDSO flow ratio of 1 000 ∶ 1 ∶ 40. SEM observations revealed a decrease in film thickness with increasing substrate temperature, decreasing from 242 nm at 25 ℃ to 156 nm at 200 ℃. Pencil hardness tests demonstrated an improvement in hardness from initial grade B to 4H. Cross-cut adhesion tests showed class 1 adhesion at 25 and 50 ℃, with improved adhesion to class 0 at higher temperatures. HCl corrosion experiments indicated that the films deposited at 200 ℃ demonstrated improved corrosion resistance. These findings provide new insights for surface treatment technology in specific application scenarios, particularly highlighting the temperature-dependent optimization of film properties.

References

[1] He Q, Xu Y, Zhang F Y, et al. Preparation methods and research progress of superhydrophobic anti-icing surface [J]. *Advances in Colloid and Interface Science*, 2024, 323: 103069.

[2] Liu Y, Cheng L L, Liu Y H, et al. Interfacial connection and service performance of CFRP-6061 aluminum alloy enhanced by laser plasma co-treatment [J]. *Journal of Donghua University (English Edition)*, 2025, 42(4): 358-370.

[3] Huang M L, Wu Y Z, Lu S G. Structural coloration and ultraviolet protective fabrication on fabrics coated with SiO_2/TiO_2 multilayer films via a magnetron sputtering method [J]. *Journal of Industrial Textiles*, 2022, 52: 15280837221114636.

[4] Afrida N R, Wang Y M, Zhou C, et al. Effect of SiO_2 nanoparticles on durability of polyurethane-coated polyamide tent fabric [J]. *Journal of Donghua University (English Edition)*, 2025, 42(6): 620-627.

[5] Zhao D Q, Xu F, Wang G G, et al. SiO_2/HfO_2 laser film with enhanced protection and antireflection for sapphire infrared windows at high temperatures [J]. *ACS Applied Electronic Materials*, 2021, 3(10): 4611-4617.

[6] Yang J Y, Xu F. Preparation and properties of organic-inorganic composite hydrophobic silica films [J]. *Sciences of Conservation and Archaeology*, 2018, 30(2): 10-19. (in Chinese)

[7] Xie W C, Zhou Y J, Chu Z Y, et al. Effect of surface modification on antioxidation behavior of iron fiber [J]. *Materials Protection*, 2005(8): 5-8, 69. (in Chinese)

[8] Feng X J, Shi Y L, Yin X L, et al. Transparent superhydrophobic film with anti-fouling and anti-scaling ability by facile method of dip-coating SiO_2 sol [J]. *Materials Research Express*, 2022, 9(1): 016404.

[9] Gasiorek J, Mazur-Nowacka A, Szczurek A, et al. Influence of zirconia and organic additives on mechanical and electrochemical properties of silica sol-gel coatings [J]. *Materials*, 2021, 14(9): 2389.

[10] Zhao C J, Zhao L R, Liu J C, et al. Effect of sputtering power on the properties of SiO_2 films grown by radio frequency magnetron sputtering at room temperature [J]. *Optical and Quantum Electronics*, 2021, 53(1): 15.

[11] Sheriff M A, Hashim M R, Pakhuruddin M Z. Effect of deposition time toward surface morphological and optical properties of silicon dioxide thin films on black silicon by liquid-phase deposition [J]. *Applied Physics A*, 2022, 128(8): 674.

[12] Jiang H Y, Wu J Y, Wen Z Y, et al. Surface doping and humidity sensing of MoS_2 field-effect transistor by oxygen plasma treatment [J]. *Journal of Donghua University (English Edition)*, 2024, 41(2): 130-136.

[13] Wang J H, Wang T, Wang X, et al. Effect of applied voltage on localized deposition of silicon dioxide-like films on stainless steel using atmospheric pressure microplasma jet [J]. *Plasma Chemistry and Plasma Processing*, 2023, 43(4): 879-899.

[14] Yu F L, Bai Y, Qin Y, et al. Influence of substrate temperature on the morphology, composition and growth rate of SiC films deposited by PECVD [J]. *Journal of Inorganic Materials*, 2013, 28(2): 201-206. (in Chinese)

[15] Hu X H, Li F S, Wu Z X, et al. Effect of substrate temperature on preparation of large area organic solar cell array by spraying [J]. *Chinese Journal of Luminescence*, 2013, 34(12): 1641-1645. (in Chinese)

[16] Jin Y J, Guo Y, Han Q H, et al. Study on the dynamics and characteristics of atmospheric pulsed discharge assisted by AC sinusoidal voltage [J]. *Journal of Donghua University (Natural Science)*, 2023, 49(3): 149-153. (in Chinese)

[17] Zhao Y L, Yu Z X, Planche M P, et al. Influence of substrate properties on the formation of suspension plasma sprayed coatings [J]. *Journal of Thermal Spray Technology*, 2018, 27(1/2): 73-83.

[18] Xu L G, Geng Z, He J H, et al. Mechanically robust, thermally stable, broadband antireflective, and superhydrophobic thin films on glass substrates [J]. *ACS Applied Materials & Interfaces*, 2014, 6(12): 9029-9035.

[19] Zhang D, Ke P L, Wang A Y, et al. Properties of functional decorative silicon oxide films prepared by PECVD [J]. *Chinese Journal of Materials Research*, 2019, 33(6): 467-474. (in Chinese)

[20] Smith D L. Thin-film deposition: principles and practice [M]. New York: McGraw-Hill, 1995.

基底温度对等离子体射流制备类 SiO_2 薄膜的影响

张娇娇[1]，徐　雨[1,2,3*]，钱智欣[1]，黄晓江[1,2,3]

1. 东华大学 物理学院，上海 201620
2. 东华大学 磁约束核聚变教育部研究中心，上海 201620
3. 东华大学 纺织行业先进等离子体技术与应用重点实验室，上海 201620

摘　要：探讨了基底温度(25~200 ℃)对常压等离子体射流制备类 SiO_2 薄膜的影响。在高温下沉积的薄膜厚度有所减小(从 242 nm 降至 156 nm)，但机械和化学性能得到增强，铅笔硬度从 B 提高到 4H。基底温度不低于 100 ℃时制备的薄膜附着力提高到 0 级（无脱落）。X 射线光电子能谱证实，基底温度从 25 ℃升至 200 ℃，所制得的薄膜的碳含量减少，SiO_2 含量增加，表明前驱体分解加剧。盐酸腐蚀测试(浸渍 3.0 h)表明，基底温度为 200 ℃时制备的薄膜耐腐蚀性增强，质量损失 6.53%，而无涂层对照组质量损失 7.01%。结果表明，基底温度是制备应用于腐蚀性环境中的防护涂层的关键工艺参数。

关键词：大气压等离子体射流；放电；薄膜；基底温度；耐腐蚀性能；SiO_2